International Conference on Mathematics, Computational Methods & Reactor Physics (M&C 2009)
Saratoga Springs, New York, May 3-7, 2009, on CD-ROM, American Nuclear Society, LaGrange Park, IL (2009)

ASYMPTOTIC ANALYSIS OF SPATIAL DISCRETIZATIONS IN IMPLICIT MONTE CARLO

Jeffery D. Densmore
Computational Physics and Methods Group, Los Alamos National Laboratory
P.O. Box 1663, MS D409, Los Alamos, NM 87545, USA
jdd@lanl.gov

ABSTRACT

We perform an asymptotic analysis of spatial discretizations in Implicit Monte Carlo (IMC). We consider two asymptotic scalings: one that represents a time step that resolves the mean-free time, and one that corresponds to a fixed, optically large time step. We show that only the latter scaling results in a valid spatial discretization of the proper diffusion equation, and thus we conclude that IMC only yields accurate solutions when using optically large spatial cells if time steps are also optically large. We demonstrate the validity of our analysis with a set of numerical examples.

Key Words: Asymptotic analysis; Implicit Monte Carlo; Hybrid methods

1. INTRODUCTION

Two important asymptotic limits in transport theory are the asymptotic diffusion limit for linear radiation transport [1–3] and the asymptotic equilibrium diffusion limit for nonlinear radiative transfer [4]. These limits represent the situation where the particle mean-free path and, in the case of time-dependent problems, mean-free time are small with respect to the typical length and time scales upon which the solution varies. Away from problem boundaries and initial times, the leading-order asymptotic solutions in these two limits are described by the linear diffusion equation and the equilibrium diffusion equation, respectively.

Asymptotic analysis is a powerful method for investigating the behavior of discretization schemes in the asymptotic limits discussed above [5–7]. In this technique, the leading-order asymptotic solution of the equations corresponding to a particular discretization method is determined. If this solution satisfies a valid discretization of the appropriate diffusion equation, then we say that the method "has the diffusion limit." Discretization schemes that have the diffusion limit yield accurate results, even if spatial cells and time steps are optically large (i.e., large with respect to the mean-free path and mean-free time), as long as the spatial and temporal variations of the solution are resolved. If a discretization scheme does not have the diffusion limit, then optically small spatial cells and time steps must be used to generate accurate solutions. Asymptotic analysis has been successfully applied to both discrete-ordinates and Monte Carlo methods, for example in Refs. [8–12].

In this paper, we perform an asymptotic analysis of spatial discretizations in Implicit Monte Carlo (IMC) [13], a Monte Carlo technique for solving nonlinear radiative-transfer problems. Unlike standard Monte Carlo, IMC employs both spatial and temporal discretizations and linearizations because of the nonlinear nature of these types of problems. In this sense, IMC is a hybrid method

that combines Monte Carlo and deterministic techniques. Densmore and Larsen have previously examined the temporal discretizations and linearizations through asymptotic analysis [12]. Here, we specifically investigate the approximation of radiation absorption and re-emission in IMC by a spatially continuous artificial-scattering process and a piecewise-constant emission source within each spatial cell. For simplicity, we perform our analysis using a steady-state, linear radiation-transport problem with scattering serving as a surrogate for absorption and re-emission. This approach is similar to that taken by Clouët and Samba [11] in their examination of the Symbolic Implicit Monte Carlo method [14, 15]. To model the spatial discretization of radiation absorption and re-emission, we split scattering into spatially continuous and piecewise-constant components. We consider two asymptotic scalings: one that represents a time step that resolves the mean-free time, and one that corresponds to a fixed, optically large time step. Although the time step is optically small in the former scaling, spatial cells remain optically large and an asymptotic analysis is still appropriate. We will show that only the latter scaling results in a valid discretization of the linear diffusion equation, and thus we conclude that IMC only yields accurate solutions with optically large spatial cells when time steps are also optically large. This behavior has been observed numerically by McKinley, Brooks, and Szoke [16]. In our work, we explain this deficiency of IMC using asymptotic analysis.

We begin the remainder of this paper with a brief review of nonlinear radiative transfer and IMC. Next, we introduce our model problem and describe how we represent the spatial discretization of radiation absorption and re-emission through scattering. We then perform an asymptotic analysis of this model problem under both scalings. Next, we present a set of numerical examples that test the validity of our analysis. We conclude with a brief discussion.

2. RADIATIVE TRANSFER AND IMPLICIT MONTE CARLO

In the absence of internal sources and scattering, the frequency-independent, planar-geometry, nonlinear radiative-transfer equations are [17–19]

$$\frac{1}{c}\frac{\partial I}{\partial t}+\mu\frac{\partial I}{\partial x}+\sigma I=\frac{1}{2}\sigma acT^4 \quad , \tag{1}$$

and

$$\frac{\partial U}{\partial t}=\sigma\int_{-1}^{1}Id\mu-\sigma acT^4 \quad . \tag{2}$$

Here, $0<x<X$ is the spatial variable, $-1\leq\mu\leq1$ is the angular variable, $t>0$ is the temporal variable, $I(x,\mu,t)$ is the radiation intensity, $T(x,t)$ is the material temperature, $\sigma(x,T)$ is the opacity, a is the radiation constant, and c is the speed of light. In addition, the material energy density $U(x,t)$ is related to the material temperature by

$$\frac{\partial U}{\partial T}=C_v \quad , \tag{3}$$

where $C_v(x,T)$ is the heat capacity. Appropriate boundary and initial conditions also accompany Eqs. (1) and (2).

To solve Eqs. (1) and (2) using IMC, we first prescribe a spatial grid
$0=x_{1/2}<x_{3/2}<x_{5/2}<\cdots<x_{J+1/2}=X$ consisting of J cells and a temporal grid

$0 = t_0 < t_1 < t_2 < \cdots$. Then, within each spatial cell $x_{j-1/2} < x < x_{j+1/2}$ and time step $t_n < t \leq t_{n+1}$, the IMC simulation is governed by [13]

$$\frac{1}{c}\frac{\partial I}{\partial t} + \mu\frac{\partial I}{\partial x} + \sigma_{n,j} I = \frac{1}{2}(1 - f_{n,j})\sigma_{n,j}\int_{-1}^{1} I(x,\mu',t)d\mu' + \frac{1}{2} f_{n,j}\sigma_{n,j} acT_{n,j}^4 \quad , \tag{4}$$

and

$$\frac{dU_j}{dt} = \frac{1}{\Delta x_j} f_{n,j}\sigma_{n,j}\int_{x_{j-1/2}}^{x_{j+1/2}}\int_{-1}^{1} I d\mu dx - f_{n,j}\sigma_{n,j} acT_{n,j}^4 \quad . \tag{5}$$

In Eqs. (4) and (5), the subscript n denotes quantities evaluated with the beginning-of-time-step value of the material temperature and the subscript j denotes cell-averaged quantities. In addition, the *Fleck factor* $f_{n,j}$ is

$$f_{n,j} = \frac{1}{1 + \alpha\beta_{n,j}\sigma_{n,j} c\Delta t_n} \quad , \tag{6}$$

where $0 \leq \alpha \leq 1$ is a user-selectable parameter and

$$\beta_{n,j} = \frac{4aT_{n,j}^3}{C_{v,n,j}} \quad . \tag{7}$$

Also, $\Delta t_n = t_{n+1} - t_n$ is the time-step size and $\Delta x_j = x_{j+1/2} - x_{j-1/2}$ is the cell width.

We can determine the radiation intensity from Eq. (4) each time step using standard Monte Carlo methods. At the end of each time step, we can update the material temperature and energy density through Eqs. (3) and (5). By comparing Eqs. (1) and (4), we see that the emission source on the right side of Eq. (1) is approximated in IMC with artificial scattering and a piecewise-constant emission source. Thus, when a particle undergoes a collision it either isotropically scatters, which represents absorption and re-emission within a time step, or is absorbed. If a particle is absorbed, its energy is added to the material energy in the spatial cell where the absorption took place, and this energy can be subsequently re-emitted in a later time step. However, when this energy is re-emitted, the initial position of the new particle is not the same as where the original particle was absorbed, but is sampled uniformly within the spatial cell. Of course, particles that artificially scatter do not suffer from this spatial discretization as scattering does not alter the position of a particle. It is this approximation of absorption and re-emission by spatially continuous and piecewise-constant components that we address in this paper.

3. MODEL PROBLEM

For simplicity, we now represent Eqs. (1) and (2) using a steady-state, homogeneous, linear radiation-transport problem,

$$\mu\frac{\partial \psi}{\partial x} + \Sigma_t \psi = \frac{\Sigma_s}{2}\int_{-1}^{1}\psi(x,\mu')d\mu' + \frac{Q}{2} \quad . \tag{8}$$

Here, $\psi(x,\mu)$ is the angular flux, Σ_t is the total cross section, Σ_s is the scattering cross section, Q is the radiation source, and the definitions of x and μ still hold. Three other important quantities are the scalar flux,

$$\phi(x) = \int_{-1}^{1}\psi(x,\mu)d\mu \quad , \tag{9}$$

the current,

$$J(x) = \int_{-1}^{1} \mu\psi(x,\mu)d\mu \quad , \tag{10}$$

and the absorption cross section,

$$\Sigma_a = \Sigma_t - \Sigma_s \quad . \tag{11}$$

Along with Eq. (8), we impose isotropic boundary conditions,

$$\psi(0,\mu) = \frac{\phi_L}{2} \quad , \quad 0 < \mu \leq 1 \quad , \tag{12}$$

and

$$\psi(X,\mu) = \frac{\phi_R}{2} \quad , \quad -1 \leq \mu < 0 \quad , \tag{13}$$

where ϕ_L and ϕ_R are the scalar fluxes corresponding to the incident angular fluxes at the left and right problems boundaries, respectively. Equation (8) represents Eqs. (1) and (2) in the sense that scattering serves as a surrogate for absorption and re-emission.

To model the spatial discretization of absorption and re-emission in Eq. (4), we split the scattering in Eq. (8) into spatially continuous and piecewise-constant components. If we again prescribe an appropriate spatial grid, then within each cell we have

$$\mu\frac{\partial\psi}{\partial x} + \Sigma_t\psi = \frac{\Sigma_s}{2}\left[(1-f)\int_{-1}^{1}\psi(x,\mu')d\mu' + \frac{f}{\Delta x_j}\int_{x_{j-1/2}}^{x_{j+1/2}}\int_{-1}^{1}\psi(x',\mu')d\mu'dx'\right] + \frac{Q}{2} \quad . \tag{14}$$

In this expression, $0 \leq f \leq 1$ represents the Fleck factor, but is a quantity of our choosing instead of being defined by Eq. (6). This modified transport equation is amenable to Monte Carlo simulation: each time a particle scatters, with probability f a new position is sampled uniformly within the current spatial cell.

4. ASYMPTOTIC ANALYSIS

The asymptotic diffusion limit is described by the following scaled cross sections and radiation source [1–3]:

$$\Sigma_t = \frac{\sigma_t}{\epsilon} \quad ; \tag{15}$$

$$\Sigma_a = \epsilon\sigma_a \quad ; \tag{16}$$

$$Q = \epsilon q \quad . \tag{17}$$

Here, σ_t, σ_a, and q are constant $O(1)$ quantities and $\epsilon \ll 1$. Under this scaling, the asymptotic solution of Eqs. (8), (12), and (13) [1–3] shows that, to leading order in ϵ, the angular flux is isotropic,

$$\psi = \frac{\phi}{2} \quad , \tag{18}$$

while the scalar flux satisfies a linear diffusion equation,

$$-\frac{1}{3\sigma_t}\frac{d^2\phi}{dx^2} + \sigma_a\phi = q \quad , \tag{19}$$

with boundary conditions of the form

$$\phi(0) = \phi_L \quad , \tag{20}$$

and

$$\phi(X) = \phi_R \quad . \tag{21}$$

Asymptotic solutions of this type are typically only valid away from problem boundaries. However, because we have specified isotropic boundary conditions in Eqs. (12) and (13), the leading-order solution given by Eqs. (18)–(21) holds both in the problem interior and near problem boundaries, as well.

We now perform an asymptotic analysis of Eq. (14). In this analysis, we develop a leading-order asymptotic solution of this expression and Eqs. (12) and (13) under the scaling in Eqs. (15)–(17). Ideally, this solution should yield a valid spatial discretization of Eqs. (18)–(21). We begin by evaluating Eq. (14) with Eqs. (11) and (15)–(17) to write

$$\epsilon\mu\frac{\partial\psi}{\partial x} + \sigma_t\psi = \frac{1}{2}\left(\sigma_t - \epsilon^2\sigma_a\right)\left[(1-f)\int_{-1}^{1}\psi(x,\mu')d\mu' + f\phi_j\right] + \epsilon^2\frac{q}{2} \quad . \tag{22}$$

In Eq. (22), we have defined the cell-averaged scalar flux as

$$\begin{aligned}\phi_j &= \frac{1}{\Delta x_j}\int_{x_{j-1/2}}^{x_{j+1/2}}\phi(x)dx \\ &= \frac{1}{\Delta x_j}\int_{x_{j-1/2}}^{x_{j+1/2}}\int_{-1}^{1}\psi(x,\mu)d\mu dx \quad .\end{aligned} \tag{23}$$

Next, we express the angular flux in two different ways. Away from cell edges, we employ an "interior" solution,

$$\psi(x,\mu) = \psi^{(i)}(x,\mu) \quad . \tag{24}$$

Near each cell edge $x_{j+1/2}$, we represent the angular flux with a "boundary-layer" solution,

$$\psi(x,\mu) = \psi^{(b)}_{j+1/2}(z,\mu) \quad , \tag{25}$$

where z is a local "fast" spatial variable defined as

$$z = \frac{\sigma_t}{\epsilon}(x - x_{j+1/2}) \quad . \tag{26}$$

The interior and boundary-layer solutions are related by the following matching conditions:

$$\lim_{x\to x^-_{j+1/2}}\psi^{(i)} = \lim_{z\to-\infty}\psi^{(b)}_{j+1/2} \quad , \quad 1 \le j \le J \quad ; \tag{27}$$

$$\lim_{x\to x^+_{j+1/2}}\psi^{(i)} = \lim_{z\to+\infty}\psi^{(b)}_{j+1/2} \quad , \quad 0 \le j \le J-1 \quad . \tag{28}$$

In addition, at the problem boundaries $x_{1/2}$ and $x_{J+1/2}$, the boundary-layer solutions satisfy the boundary conditions specified in Eqs. (12) and (13),

$$\psi^{(b)}_{1/2}(0,\mu) = \frac{\phi_L}{2} \quad , \quad 0 < \mu \le 1 \quad , \tag{29}$$

and

$$\psi^{(b)}_{J+1/2}(0,\mu) = \frac{\phi_R}{2} \quad , \quad -1 \leq \mu < 0 \quad . \tag{30}$$

We continue by expressing the interior and boundary-layer solutions and the cell-averaged scalar flux using asymptotic power series in ϵ,

$$\psi^{(i)}(x,\mu) \sim \sum_{k=0}^{\infty} \epsilon^k \psi^{(i,k)}(x,\mu) \quad , \tag{31}$$

$$\psi^{(b)}_{j+1/2}(z,\mu) \sim \sum_{k=0}^{\infty} \epsilon^k \psi^{(b,k)}_{j+1/2}(z,\mu) \quad , \tag{32}$$

and

$$\phi_j \sim \sum_{k=0}^{\infty} \epsilon^k \phi_j^{(k)} \quad . \tag{33}$$

Applying Eqs. (9) and (10) to Eqs. (31) and (32) yields similar representations of the interior and boundary-layer scalar flux and current. To develop a set of equations for $\psi^{(i,k)}$ and $\psi^{(b,k)}_{j+1/2}$, we substitute Eqs. (31)–(33) into Eqs. (22) and (27)–(30) and equate terms that are of the same order in ϵ. We can then determine an expression for $\phi_j^{(k)}$ with these results and Eq. (23).

We also consider two different scalings of f. In the asymptotic equilibrium diffusion limit [4], the mean-free time is an $O(\epsilon^2)$ quantity, while the Fleck factor given by Eq. (6) scales as [12]

$$f_{n,j} = \frac{\epsilon^2}{\epsilon^2 + C_{n,j}\Delta t_n} \quad , \tag{34}$$

where $C_{n,j}$ is an $O(1)$ quantity. If a time step is chosen that resolves the mean-free time, then Δt_n must also scale as $O(\epsilon^2)$, and we see from Eq. (34) that the Fleck factor is an $O(1)$ quantity. In this case, we represent f using

$$f = f^{(0)} \quad . \tag{35}$$

In contrast, if the time step is fixed (i.e., it is not a function of ϵ) and therefore optically large, then Δt_n is an $O(1)$ quantity, and Eq. (34) shows that Fleck factor scales as $O(\epsilon^2)$. To model this situation, we express f as

$$f = \epsilon^2 f^{(2)} \quad . \tag{36}$$

4.1. $O(1)$ Fleck Factor

We first examine the case where f is described by Eq. (35). Evaluating Eq. (22) with Eqs. (31) and (33) reveals that the $O(1)$ equation is

$$\sigma_t \psi^{(i,0)} = \frac{\sigma_t}{2}\left[\left(1 - f^{(0)}\right)\int_{-1}^{1} \psi^{(i,0)}(x,\mu')d\mu' + f^{(0)}\phi_j^{(0)}\right] \quad . \tag{37}$$

When we integrate this expression over angle and solve for the leading-order interior scalar flux, we have

$$\phi^{(i,0)} = \phi_j^{(0)} \quad . \tag{38}$$

Thus, the leading-order interior scalar flux is piecewise constant and equal to the leading-order cell-averaged scalar flux in each spatial cell. Combining Eqs. (37) and (38) yields

$$\psi^{(i,0)} = \frac{\phi_j^{(0)}}{2} \quad , \tag{39}$$

which is a valid form of Eq. (18).

We continue by considering an interior cell edge $x_{j+1/2}$, where $1 \leq j \leq J-1$. Substituting Eqs. (32) and (33) into Eq. (22) and making use of Eq. (26) gives the $O(1)$ equation in cell j as

$$\mu \frac{\partial}{\partial z} \psi_{j+1/2}^{(b,0)} + \psi_{j+1/2}^{(b,0)} = \frac{1-f^{(0)}}{2} \int_{-1}^{1} \psi_{j+1/2}^{(b,0)}(z,\mu') d\mu' + \frac{f^{(0)} \phi_j^{(0)}}{2} \quad , \tag{40}$$

and in cell $j+1$ as

$$\mu \frac{\partial}{\partial z} \psi_{j+1/2}^{(b,0)} + \psi_{j+1/2}^{(b,0)} = \frac{1-f^{(0)}}{2} \int_{-1}^{1} \psi_{j+1/2}^{(b,0)}(z,\mu') d\mu' + \frac{f^{(0)} \phi_{j+1}^{(0)}}{2} \quad . \tag{41}$$

Equations (40) and (41) correspond to $z < 0$ and $z > 0$, respectively. Thus, these expressions represent a nondimensional two-adjacent-half-spaces problem, where the half-spaces have the same scattering ratio $\omega = 1 - f^{(0)}$ but different sources. By inspecting Eqs. (40) and (41), we see that the leading-order boundary-layer solution has the properties

$$\lim_{z \to -\infty} \psi_{j+1/2}^{(b,0)} = \frac{\phi_j^{(0)}}{2} \quad , \tag{42}$$

and

$$\lim_{z \to +\infty} \psi_{j+1/2}^{(b,0)} = \frac{\phi_{j+1}^{(0)}}{2} \quad . \tag{43}$$

Comparing Eqs. (42) and (43) to Eq. (39) shows that the matching conditions in Eqs. (27) and (28) are satisfied to leading order. In addition, we can relate the leading-order boundary-layer scalar flux to the leading-order boundary-layer current at the interface between the two half-spaces (i.e., $z = 0$) by integrating Eqs. (40) and (41) over space and angle and applying Eqs. (42) and (43). This process yields

$$f^{(0)} \int_{-\infty}^{0} \left(\phi_{j+1/2}^{(b,0)} - \phi_j^{(0)} \right) dz = -J_{j+1/2}^{(b,0)}(0) \quad , \tag{44}$$

and

$$f^{(0)} \int_{0}^{+\infty} \left(\phi_{j+1/2}^{(b,0)} - \phi_{j+1}^{(0)} \right) dz = J_{j+1/2}^{(b,0)}(0) \quad . \tag{45}$$

However, for this two-adjacent-half-spaces problem, the current at the interface is proportional to the difference between the sources in each half-space,

$$J_{j+1/2}^{(b,0)}(0) = \eta \left(1 - f^{(0)}\right) \left(f^{(0)} \, \phi_j^{(0)} - f^{(0)} \phi_{j+1}^{(0)} \right) \quad . \tag{46}$$

Here, $\eta(\omega)$ is a function of the scattering ratio ω and can be calculated analytically [20]. When we evaluate Eqs. (44) and (45) with Eq. (46), we have

$$\int_{-\infty}^{0} \left(\phi_{j+1/2}^{(b,0)} - \phi_j^{(0)} \right) dz = -\eta \left(1 - f^{(0)}\right) \left(\phi_j^{(0)} - \phi_{j+1}^{(0)} \right) \quad , \tag{47}$$

and

$$\int_0^{+\infty} \left(\phi_{j+1/2}^{(b,0)} - \phi_{j+1}^{(0)} \right) dz = \eta \left(1 - f^{(0)} \right) \left(\phi_j^{(0)} - \phi_{j+1}^{(0)} \right) \quad . \tag{48}$$

In a manner similar to the development of Eqs. (40) and (41), the $O(1)$ equation corresponding to the left problem boundary $x_{1/2}$ is

$$\mu \frac{\partial}{\partial z} \psi_{1/2}^{(b,0)} + \psi_{1/2}^{(b,0)} = \frac{1 - f^{(0)}}{2} \int_{-1}^{1} \psi_{1/2}^{(b,0)}(z, \mu') d\mu' + \frac{f^{(0)} \phi_1^{(0)}}{2} \quad , \tag{49}$$

where $z > 0$. Also, we see from Eqs. (29) and (32) that the $O(1)$ boundary condition is given by

$$\psi_{1/2}^{(b,0)}(0, \mu) = \frac{\phi_L}{2} \quad , \quad 0 < \mu \leq 1 \quad . \tag{50}$$

Equations (49) and (50) describe a nondimensional half-space problem with both a source and an incident angular flux. Again, the leading-order boundary-layer solution satisfies

$$\lim_{z \to +\infty} \psi_{1/2}^{(b,0)} = \frac{\phi_1^{(0)}}{2} \quad , \tag{51}$$

and consequently the matching condition in Eq. (28), as well. Integrating Eq. (49) over space and angle and making use of Eq. (51) allows us to write an expression that is equivalent to Eq. (45),

$$f^{(0)} \int_0^{+\infty} \left(\phi_{1/2}^{(b,0)} - \phi_1^{(0)} \right) dz = J_{1/2}^{(b,0)}(0) \quad . \tag{52}$$

For this half-space problem, we can show that the current at the problem boundary is of the form

$$J_{1/2}^{(b,0)}(0) = \frac{1 - A\left(1 - f^{(0)}\right)}{4} \left(\phi_L - \phi_1^{(0)} \right) \quad , \tag{53}$$

where $A(\omega)$ is the albedo for an isotropic angular flux incident upon a half-space with a scattering ratio of ω. Combining Eqs. (52) and (53) yields

$$\int_0^{+\infty} \left(\phi_{1/2}^{(b,0)} - \phi_1^{(0)} \right) dz = \frac{1 - A\left(1 - f^{(0)}\right)}{4 f^{(0)}} \left(\phi_L - \phi_1^{(0)} \right) \quad . \tag{54}$$

A similar analysis of the right problem boundary $x_{J+1/2}$ results in

$$\int_{-\infty}^{0} \left(\phi_{J+1/2}^{(b,0)} - \phi_J^{(0)} \right) dz = \frac{1 - A\left(1 - f^{(0)}\right)}{4 f^{(0)}} \left(\phi_R - \phi_J^{(0)} \right) \quad . \tag{55}$$

To calculate the leading-order cell-averaged scalar flux, we write the $O(1)$ version of Eq. (23) as

$$\phi_j^{(0)} = \frac{1}{\Delta x_j} \left[\int_0^{+\infty} \left(\phi_{j-1/2}^{(b,0)} - \phi^{(i,0)} \right) dz + \int_{x_{j-1/2}}^{x_{j+1/2}} \phi^{(i,0)} dx + \int_{-\infty}^{0} \left(\phi_{j+1/2}^{(b,0)} - \phi^{(i,0)} \right) dz \right] \quad . \tag{56}$$

The first term on the right side of Eq. (56) is the contribution from the boundary-layer solution near the left edge of the spatial cell, the second term is the contribution from the interior solution, and the third term is the contribution from the boundary-layer solution near the right edge of the spatial cell. Note that we integrate the leading-order interior scalar flux over the entire cell width instead of just away from the cell edges. For this reason, when integrating the leading-order boundary-layer scalar flux, we subtract the leading-order interior scalar flux to avoid "double counting" this quantity. Substituting Eq. (38) into Eq. (56) gives

$$\frac{1}{\Delta x_j}\left[\int_0^{+\infty}\left(\phi_{j-1/2}^{(b,0)}-\phi_j^{(0)}\right)dz+\int_{-\infty}^{0}\left(\phi_{j+1/2}^{(b,0)}-\phi_j^{(0)}\right)dz\right]=0 \quad . \tag{57}$$

When we evaluate Eq. (57) with Eqs. (47), (48), (54), and (55), we have

$$\frac{\eta\left(1-f^{(0)}\right)}{\Delta x_j}\left(\phi_{j-1}^{(0)}-2\phi_j^{(0)}+\phi_{j+1}^{(0)}\right)=0 \quad , \quad 2\leq j\leq J-1 \quad , \tag{58}$$

$$\frac{1}{\Delta x_1}\left\{\frac{1-A\left(1-f^{(0)}\right)}{4f^{(0)}}\phi_L-\left[\frac{1-A\left(1-f^{(0)}\right)}{4f^{(0)}}+\eta\left(1-f^{(0)}\right)\right]\phi_1^{(0)} + \eta\left(1-f^{(0)}\right)\phi_2^{(0)}\right\}=0 \quad , \tag{59}$$

and

$$\frac{1}{\Delta x_J}\left\{\eta\left(1-f^{(0)}\right)\phi_{J-1}^{(0)}-\left[\eta\left(1-f^{(0)}\right)+\frac{1-A\left(1-f^{(0)}\right)}{4f^{(0)}}\right]\phi_J^{(0)} + \frac{1-A\left(1-f^{(0)}\right)}{4f^{(0)}}\phi_R\right\}=0 \quad . \tag{60}$$

Equations (58)–(60) form a system of J equations for the leading-order cell-averaged scalar flux. However, in general these equations do not represent a valid spatial discretization of Eqs. (19)–(21) because they do not depend on the cross sections or radiation source. Thus, we conclude that Eq. (14) does not have the diffusion limit if f is an $O(1)$ quantity.

4.2. $O\left(\epsilon^2\right)$ Fleck Factor

When f scales as in Eq. (36), the asymptotic analysis of Eq. (14) is nearly identical to the development of Eqs. (18)–(21) [1–3], and thus we only state the major results. The leading-order interior solution is again isotropic,

$$\psi^{(i,0)}=\frac{\phi^{(i,0)}}{2} \quad , \tag{61}$$

while the leading-order interior scalar flux in each spatial cell is described by a diffusion equation of the form

$$-\frac{1}{3\sigma_t}\frac{d^2}{dx^2}\phi^{(i,0)}+\left(\sigma_a+f^{(2)}\sigma_t\right)\phi^{(i,0)}=f^{(2)}\sigma_t\phi_j^{(0)}+q \quad . \tag{62}$$

In addition, an examination of the boundary-layer solution at each cell edge yields the following:

1. The leading-order interior solution holds throughout the problem domain, including near cell edges.

2. The leading-order interior scalar flux and its derivative are continuous at interior cell edges,

$$\lim_{x \to x_{j+1/2}^-} \phi^{(i,0)} = \lim_{x \to x_{j+1/2}^+} \phi^{(i,0)} \quad , \quad 1 \leq j \leq J-1 \quad , \tag{63}$$

and

$$\lim_{x \to x_{j+1/2}^-} \frac{d}{dx}\phi^{(i,0)} = \lim_{x \to x_{j+1/2}^+} \frac{d}{dx}\phi^{(i,0)} \quad , \quad 1 \leq j \leq J-1 \quad . \tag{64}$$

3. The boundary conditions for the leading-order interior scalar flux are

$$\phi^{(i,0)}(0) = \phi_L \quad , \tag{65}$$

and

$$\phi^{(i,0)}(X) = \phi_R \quad . \tag{66}$$

The first item above allows us to write the leading-order cell-averaged scalar flux using Eq. (23) as

$$\phi_j^{(0)} = \frac{1}{\Delta x_j} \int_{x_{j-1/2}}^{x_{j+1/2}} \phi^{(i,0)} dx \quad . \tag{67}$$

Combining Eqs. (62) and (67) gives

$$-\frac{1}{3\sigma_t}\frac{d^2}{dx^2}\phi^{(i,0)} + \left(\sigma_a + f^{(2)}\sigma_t\right)\phi^{(i,0)} = \frac{f^{(2)}\sigma_t}{\Delta x_j} \int_{x_{j-1/2}}^{x_{j+1/2}} \phi^{(i,0)}(x')dx' + q \quad . \tag{68}$$

We can manipulate Eqs. (63)–(66) and (68) into a set of equations for the leading-order interior scalar flux. In fact, Eqs. (61), (65), (66), and (68) would be equivalent to Eqs. (18)–(21) if the following were true,

$$\phi^{(i,0)}(x) = \frac{1}{\Delta x_j} \int_{x_{j-1/2}}^{x_{j+1/2}} \phi^{(i,0)}(x')dx' \quad , \quad x_{j-1/2} < x < x_{j+1/2} \quad . \tag{69}$$

However, the right side of Eq. (69) is an accurate approximation of the left side when the spatial grid is sufficiently fine enough to resolve the spatial variations of the leading-order interior scalar flux (but not necessarily so fine that spatial cells are optically small). Therefore, for any reasonably chosen spatial grid, the spurious terms in Eq. (68) should nearly cancel each other, and consequently Eqs. (61), (63)–(66), and (68) form a valid spatial discretization of Eqs. (18)–(21). In this case, we conclude that Eq. (14) has the diffusion limit if f scales as $O(\epsilon^2)$.

5. NUMERICAL RESULTS

We now present numerical results from two test problems. These problems correspond to a nondimensional version of Eqs. (8), (12), and (13) with $X = 1$. In addition, we represent the cross sections and radiation source using Eqs. (15)–(17), where $\sigma_t = \sigma_a = 1$ and $\epsilon = 0.001$. The two problems differ in their values of ϕ_L, ϕ_R, and q. To solve these problems via Eq. (14), we

employ a spatial grid consisting of 10 equally sized cells. Also, we specify f using both Eqs. (35) and (36) with $f^{(0)} = f^{(2)} = 1/2$. For this value of $f^{(0)}$, $A = 0.146$ [21], and we can show that $\eta = 0.373$ through an analytic calculation [20].

In the first test problem, we model a radiation source and vacuum boundary conditions by setting $q = 1$ and $\phi_L = \phi_R = 0$. For these problem parameters, the solution of Eqs. (58)–(60) is identically zero. We have simulated this problem with both values of f using 100,000 particle histories and estimated the cell-averaged scalar flux in each spatial cell. The results of these calculations and the analytic solution of Eqs. (19)–(21) are displayed in Figure 1. From this plot, we see that when f is an $O(1)$ quantity, the cell-averaged scalar flux is nearly zero, as expected. Also, when f scales as $O(\epsilon^2)$, the cell-averaged scalar flux agrees well with the analytic diffusion solution.

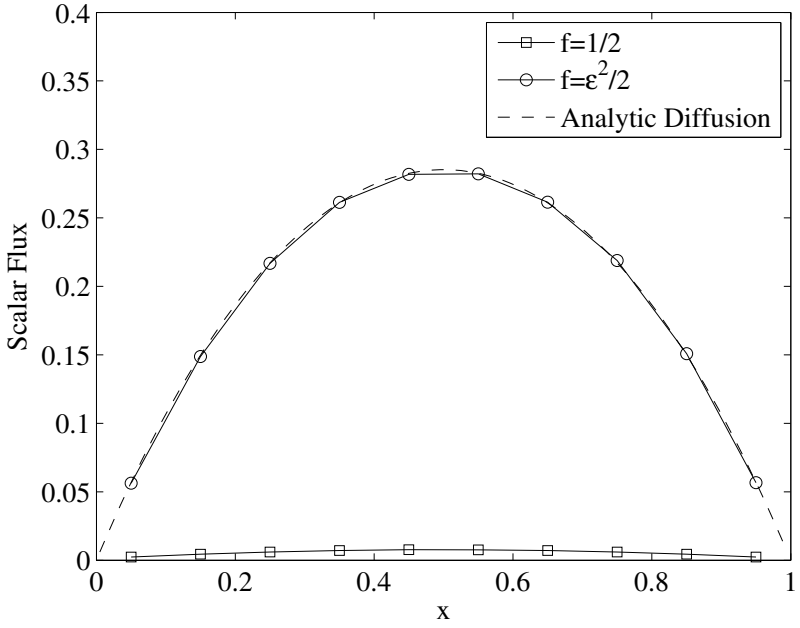

Figure 1. First Test Problem Results

The second test problem has no radiation source ($q = 0$), and the boundary conditions consist of an incident angular flux on the left problem boundary ($\phi_L = 1$) and a vacuum on the right problem boundary ($\phi_R = 0$). We have simulated this problem with both values of f using 10 million particle histories in this case and again estimated the cell-averaged scalar flux in each spatial cell. The results generated by these calculations, along with the analytic solution of Eqs. (19)–(21), are plotted in Figure 2. In addition, we have determined the "wrong" diffusion solution corresponding to Eqs. (58)–(60) and the values of A and η given above, and we include this incorrect cell-averaged scalar flux in Figure 2, as well. This figure shows that when f is an $O(1)$ quantity, the "wrong" diffusion solution is produced, while the cell-averaged scalar flux matches the analytic diffusion solution when f scales as $O(\epsilon^2)$.

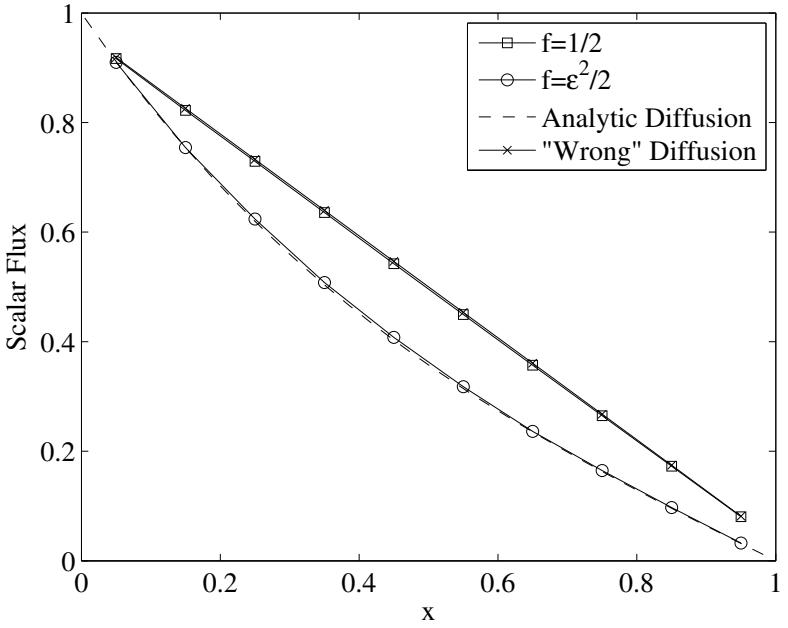

Figure 2. Second Test Problem Results

6. CONCLUSIONS

We have performed an asymptotic analysis of spatial discretizations in Implicit Monte Carlo. We have examined two asymptotic scalings: one that represents a time step that resolves the mean-free time, and one that corresponds to a fixed, optically large time step. We have shown that only under the second scaling does IMC have the diffusion limit, and thus we conclude that IMC only yields accurate results with optically large spatial cells when time steps are also optically large. We have included a set of numerical examples that demonstrate the validity of our theoretical predictions. In future work, we plan on extending our asymptotic analysis to examine an intermediate scaling that follows from a Courant limit on the time-step size [22] and "source tilting" [23], an improvement to standard IMC that models the spatial dependence of the emission source as piecewise linear instead of piecewise constant within each spatial cell.

ACKNOWLEDGMENTS

I would like to thank Jim Warsa (LANL) for helpful discussions. This work was performed under U.S. government contract DE-AC52-06NA25396 for Los Alamos National Laboratory, which is operated by Los Alamos National Security, LLC, for the U.S. Department of Energy.

REFERENCES

[1] E.W. Larsen and J.B. Keller, "Asymptotic Solution of Neutron Transport Problems for Small Mean Free Paths," *J. Math. Phys.*, **15**, 75 (1973).

[2] G.J. Habetler and B.J. Matkowsky, "Uniform Asymptotic Expansions in Transport Theory with Small Mean Free Paths, and the Diffusion Approximation," *J. Math. Phys.*, **16**, 846 (1975).

[3] E.W. Larsen, "Diffusion Theory as an Asymptotic Limit of Transport Theory for Nearly Critical Systems with Small Mean Free Paths," *Ann. Nucl. Energy*, **7**, 249 (1980).

[4] E.W. Larsen, G.C. Pomraning, and V.C. Badham, "Asymptotic Analysis of Radiative Transfer Problems," *J. Quant. Spectrosc. Radiat. Transfer*, **29**, 285 (1983).

[5] E.W. Larsen, J.E. Morel, and W.F. Miller, Jr., "Asymptotic Solutions of Numerical Transport Problems in Optically Thick, Diffusive Regimes," *J. Comp. Phys.*, **69**, 283 (1987).

[6] E.W. Larsen and J.E. Morel, "Asymptotic Solutions of Numerical Transport Problems in Optically Thick, Diffusive Regimes II," *J. Comp. Phys.*, **83**, 212 (1989).

[7] E.W. Larsen, "The Asymptotic Diffusion Limit of Discretized Transport Problems," *Nucl. Sci. Eng.*, **112**, 336 (1992).

[8] J.E. Morel, T.A. Wareing, and K. Smith, "A Linear-Discontinuous Spatial Differencing Scheme for S_n Radiative Transfer Calculations," *J. Comp. Phys.*, **128**, 445 (1996).

[9] M.L. Adams and P.F. Nowak, "Asymptotic Analysis of a Computational Method for Time- and Frequency-Dependent Radiative Transfer," *J. Comp. Phys.*, **146**, 366 (1998).

[10] M.L. Adams, "Discontinuous Finite Element Transport Solutions in Thick Diffusive Problems," *Nucl. Sci. Eng.*, **137**, 298 (2001).

[11] J.-F. Clouët and G. Samba, "Asymptotic Diffusion Limit of the Symbolic Monte-Carlo Method for the Transport Equation," *J. Comp. Phys.*, **195**, 293 (2004).

[12] J.D. Densmore and E.W. Larsen, "Asymptotic Equilibrium Diffusion Analysis of Time-Dependent Monte Carlo Methods for Grey Radiative Transfer," *J. Comp. Phys.*, **199**, 175 (2004).

[13] J.A. Fleck, Jr. and J.D. Cummings, "An Implicit Monte Carlo Scheme for Calculating Time and Frequency Dependent Radiation Transport," *J. Comp. Phys.*, **8**, 313 (1971).

[14] E.D. Brooks III, "Symbolic Implicit Monte Carlo," *J. Comp. Phys.*, **83**, 433 (1989).

[15] T. N'kaoua, "Solution of the Nonlinear Radiative Transfer Equations by a Fully Implicit Matrix Monte Carlo Method Coupled with the Rosseland Diffusion Equation via Domain Decomposition," *SIAM J. Sci. Stat. Comput.*, **12**, 505 (1991).

[16] M.S. McKinley, E.D. Brooks III, and A. Szoke, "Comparison of Implicit and Symbolic Implicit Monte Carlo Line Transport with Frequency Weight Vector Extension," *J. Comp. Phys.*, **189**, 330 (2003).

[17] G.C. Pomraning, *The Equations of Radiation Hydrodynamics*, Pergamon Press, Oxford, United Kingdom (1973).

[18] D. Mihalas and B. Weibel-Mihalas, *Foundations of Radiation Hydrodynamics*, Dover Publications, Mineola, New York (1999).

[19] J.I. Castor, *Radiation Hydrodynamics*, Cambridge University Press, Cambridge, United Kingdom (2004).

[20] K.M. Case and P.F. Zweifel, *Linear Transport Theory*, Addison-Wesley Publishing Company, Reading, Massachusetts (1967).

[21] G.C. Pomraning, "Emissivity Estimates," *J. Quant. Spectrosc. Radiat. Transfer*, **19**, 607 (1979).

[22] R.J. LeVeque, *Finite Volume Methods for Hyperbolic Problems*, Cambridge University Press, Cambridge, United Kingdom (2002).

[23] J.A. Fleck, Jr. and E.H. Canfield, "A Random Walk Procedure for Improving the Computational Efficiency of the Implicit Monte Carlo Method for Nonlinear Radiation Transport," *J. Comp. Phys.*, **54**, 508 (1984).